Solar Energy 241 (2022) 584–591

Contents lists available at ScienceDirect

Solar Energy

journal homepage: www.elsevier.com/locate/solener

Indoor validation of a multiwavelength measurement approach to estimate soiling losses in photovoltaic modules

Álvaro Fernández-Solas [a,*], Leonardo Micheli [a,b], Florencia Almonacid [a], Eduardo F. Fernández [a]

[a] Advances in Photovoltaic Technology (AdPVTech), CEACTEMA, University of Jaén (UJA), Las Lagunillas Campus, Jaén 23071, Spain
[b] Current: Department of Astronautical, Electrical and Energy Engineering (DIAEE), Sapienza University of Rome, 00184 Rome, Italy

ARTICLE INFO

Keywords:
Photovoltaic
Modeling
Soiling
Sensor
Spectral transmittance

ABSTRACT

Soiling is a factor that impacts the performance of photovoltaic (PV) modules. Nowadays, the research related to PV soiling monitoring is focused on optical sensors, which estimate the soiling loss through a monochromatic transmittance or reflectance measurement. However, these typically neglect the spectral profile of soiling transmittance, which tends to absorb shorter wavelengths more than the longer ones. This leads to a spectral red shift of the light that is transmitted to the PV cells of a module. Therefore, if the spectral component of soiling is not considered, the estimated soiling losses are not fully representative of those occurring in the real PV modules. This investigation aims to address this issue by modeling the full soiling transmittance spectrum using several monochromatic light sources in a new version of a previously presented optical soiling sensor, called "DUSST". Four different combinations of mono-wavelength light-emitting diodes have been used to model the full spectral transmittance profile of artificially soiled PV glass coupons and to estimate the electrical losses of distinct PV technologies. The results show that the errors in soiling estimation can be minimized by using an appropriate wavelength combination. The difference between the measured and the estimated soiling losses can be lower than 3% if the most convenient wavelength combination is utilized. In the case of m-Si, which is the prevalent PV technology nowadays, the application of the optimum wavelength combination is found to reduce the maximum measurement error to 2.6%, from the initial 7.7% returned when a single wavelength was employed.

1. Introduction

Soiling consists of the accumulation of dust, dirt and other contaminant particles on the photovoltaic (PV) modules surface. Its main impact is the reduction of the power output of PV systems, which directly translates into energy and economic losses (Ilse et al., 2019). Nowadays, the impact of soiling has become one of the principal concerns of the PV community, as evidenced by the large number of publications in recent years (Costa et al., 2018; Figgis et al., 2017; Song et al., 2021). Soiling on PV technology has been already investigated from different sides, which include the study of mitigation and cleaning strategies (Chanchangi et al., 2021; Eihorn et al., 2019; Ilse et al., 2019; Ravi et al., 2019; Şevik and Aktaş, 2022) and their impact on the profits (Fathi et al., 2017; Micheli et al., 2020c; Rodrigo et al., 2020). Previous research agrees that soiling mitigation has to be tailored to the specific conditions of each site, as soiling can vary depending on the location and on the season. In addition, one has to consider the angular (Burton et al., 2016; Martín and Ruiz, 2005; Zorrilla-Casanova et al., 2013) and the spectral effects (Burton et al., 2015; Burton and King, 2014; Fernández-Solas et al., 2021; John et al., 2015) of soiling on PV modules, which vary continuously throughout the day and change depending on the PV module.

For all the aforementioned reasons, soiling has to be tackled on site through the implementation of an appropriate monitoring solution (Bessa et al., 2021). Different approaches to extract and quantify the losses due to soiling have been developed. These include the direct extraction of the soiling losses from PV performance data (Deceglie et al., 2018; Micheli et al., 2021; Skomedal et al., 2019); methods that use as inputs different environmental and meteorological parameters to estimate the losses (Javed et al., 2017; Kimber et al., 2006; Micheli et al., 2020a); and the use of specialized soiling monitoring equipment, such as soiling stations (Gostein et al., 2015). These consist of two PV devices installed side-by-side within a PV plant: one of them is regularly cleaned and the other is left to naturally soil at the same conditions as the

* Corresponding author.
E-mail addresses: afsolas@ujaen.es (Á. Fernández-Solas), leonardo.micheli@uniroma1.it (L. Micheli), facruz@ujaen.es (F. Almonacid), eduardo.fernandez@ujaen.es (E.F. Fernández).

https://doi.org/10.1016/j.solener.2022.06.036
Received 27 April 2022; Received in revised form 16 June 2022; Accepted 23 June 2022
Available online 4 July 2022

modules of the plant (Gostein et al., 2014). The losses are obtained from the direct comparison of the power outputs of both modules. Soiling stations are the most common solution for monitoring soiling, but they are expensive and require careful maintenance. For this reason, one of the most recent trends to evaluate the impact of soiling is the use of optical soiling detectors, which estimate the losses from optical measurements of a PV glass coupon. These sensors do not require the sun radiation to operate as they use independent light sources. So, they do not need a reference measurement, because the intensity of the light source is known. This way, the soiling losses can be obtained instantaneously, being this aspect one of the main benefits of these sensors when compared against the above mentioned approaches.

DustIQ (Korevaar et al., 2017) and MARS (Gostein et al., 2018) were the first optical soiling sensors to be developed. DustIQ (Korevaar et al., 2017) is based on reflectance measurements. It calculates the transmittance loss of a soiled glass coupon by using a light-emitting diode (LED) and the signal received by a photodiode adhered to the glass surface. A linear correlation between the photodiode voltage, which represents the amount of reflected light from the soiled glass, and the transmittance loss is established. This way, the transmittance loss is indirectly obtained. The value of the slope varies with the color of the soiling, but is independent of the grain size. MARS (Gostein et al., 2018) estimates the soiling loss using a microscopic imaging approach. The manufacturer states that, differently from the DustIQ sensor, MARS provides results with a negligible dependence on dust color. Another optical soiling sensor, called DUSST (Fernández-Solas et al., 2020; Fernández et al., 2020) and developed by some of the authors of this study, estimates the soiling losses by measuring the monochromatic light (530 nm) that is transmitted through a naturally soiled glass coupon. The main benefit of this sensor is that it directly estimates the losses from the reduction of the transmittance caused by the presence of soiling on the surface of a PV device. The choice of the monochromatic light was accounted by a previous study (Micheli et al., 2019), which analyzed the possibility of correlating the soiling losses with transmittance measurements at a single wavelength. That work found that the soiling losses can be accurately estimated (values of coefficient of determination (R^2) higher than 0.9 were returned) for transmittances measured at wavelengths between 500 nm and 600 nm for various PV technologies. Despite the different efforts to develop soiling optical sensors, none of the currently available monitors takes into account the dependence of the spectral transmittance of soiling (Smestad et al., 2020), specially towards the blue and the ultraviolet (UV) ranges of the spectrum, where soiling causes higher transmittance drops (Qasem et al., 2014). The study presented by John et al., 2015 demonstrated that most of the soiling losses occur at the shorter wavelengths, especially those that belong to the UV and blue regions of the incident spectrum. This fact causes a red-shift of the transmitted light that reaches the PV cells. This is a key aspect as PV materials are spectrally selective and their response is known to depend on the input spectrum (Fernández et al., 2016) and on the spectral nature of soiling (Fernández et al., 2019).

To address this issue, the possibility of using several transmittance measurements at different wavelengths was theoretically analyzed by the authors in a previous study (Micheli et al., 2020b). In that work, combinations of measurements at 2 or 3 specific wavelengths were used to model the full soiling spectral transmittance profile (TPR). The present investigation aims to bring into reality the novel optical soiling sensor concept theoretically investigated in our early work. The findings of this study are here extended through an experimental investigation, conducted in a laboratory using various LEDs radiating at different wavelengths to improve the design and the performance of the previously presented DUSST sensor. Different combinations of measurements taken by commercial high power LEDs are investigated and used to model the soiling TPR through an empirical equation already described in (Smestad et al., 2020). Differently from previous works, the present paper makes use of commercial LEDs, and therefore handles with actual limitations that the previous theoretical work did not contemplate. Among these limitations, one can list: (i) the use of non-strict monochromatic LEDs, as actual commercial ones are characterized by a narrow spectral distribution around a peak wavelength; (ii) the limited variety of high power monochromatic LEDs in the market, especially of those emitting in the UV region of the spectrum due to their low efficiency, which is an issue that is still under investigation (Amano et al., 2020; Susilo et al., 2020); (iii) the influence of the different thermal drifts of LEDs within the same combination on the results, as each LED is manufactured with a different semiconductor material; and (iv) the impact of differences in the light collimation of the different LEDs due to variations in the optical refractive index with the wavelength (Saura et al., 2021). These aspects, which are expected to alter the theoretical results, can play a vital role when deciding future design improvements of the sensor, and therefore, they are the target of the present research.

2. Materials and methods

The prototype of the DUSST sensor described in (Fernández-Solas et al., 2020) and experimentally investigated in outdoors in (Muller et al., 2021) is used in this study (see Fig. 1). Originally, DUSST was designed to estimate the soiling losses through a single wavelength measurement, by correlating the current loss measured by the light detector with the transmittance loss at that specific wavelength. Herein, DUSST operates with several monochromatic high-power LEDs with distinct peak wavelengths (see Table 1) in the visible (VIS) region of the spectrum. It should be noted that the LEDs used in this study are not strictly monochromatic, as these present a narrow normal spectral distribution around the peak wavelength.

Following the same procedure employed in (Fernández-Solas et al., 2020), the first step is to calibrate the response of the sensor with the different LEDs. The transmittance loss is then converted into an electrical loss thanks to conversion factors that were obtained by using a set of screening masks with different shades of grey printed on polyester

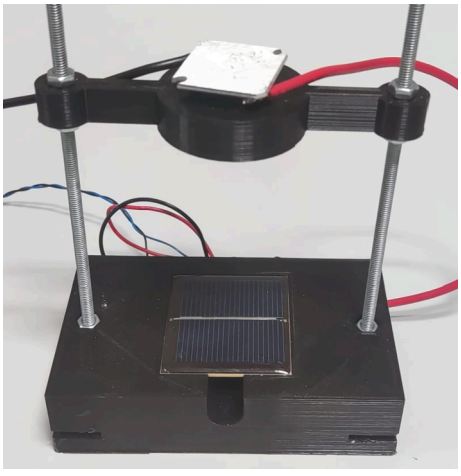

Fig. 1. DUSST prototype used in this work.

Table 1
Results of the calibration of the DUSST output for the different LEDs.

LED color	Peak wavelength [nm]	Linear Correlation (Transmittance loss = Slope × Electrical loss)	
		Slope	r
Blue	448	1.598	0.986
Green	530	1.265	0.995
Amber	591	1.349	0.992
Far Red	720	1.373	0.988

films. The hemispherical transmittance of the masks is measured using a Tungsten-Halogen light source and a Stellar Net Black-Comet spectrophotometer within the wavelength range 380 nm to 1080 nm.

Once electrical and transmittance losses have been calculated, linear correlations between them are found by using the *linregress* function in the SciPy library for Python 3.7 (Virtanen et al., 2020). The fitting is performed forcing the intercept to zero, under the assumption that no current would be produced if the soiling losses reach 100%. It should be noted that the values of the r coefficient for all the correlations are higher than 0.98, thus signifying the reliability of the fits. The values of the slopes, along with those of the r coefficients are shown in Table 1.

After obtaining the transmittance losses at the different wavelengths shown in Table 1 through the DUSST measurements and the above mentioned correlations, the empirical equation (1), introduced for the first time in Smestad et al., 2020 and based on the Angström turbidity formula (Ångström and Angstrom, 1929), is used to model the spectral TPR of soiling. This equation is here called the Three-variable single exponential (3v1e) equation:

$$T(\lambda) = e^{-\beta \bullet \lambda^{-\alpha}} + \gamma \tag{1}$$

where T(λ) is the hemispherical transmittance at a wavelength λ (in μm) and α, β and γ are wavelength independent variables. α relates to the size of the particles and β to the density of particles and to the strength of their forward scattering. γ is a factor needed to consider the different mechanisms taking place when particles are deposited instead of suspended. In the original work, the authors were able to correlate β, γ and the area covered by soiling. However, investigations are still ongoing to find a correlation for α.

In lack of this correlation, this work identifies the values of the three variables in Eq. (1) by fitting the function through the measurement of transmittance at three distinct wavelengths. Three is the minimum number of measurements needed to determine the values of the three variables. These have been extracted through the *curve_fit* function in the SciPy library for Python 3.7, which uses non-linear least-squares to fit the experimental data to a function. The initial guesses and the bounds for the variables α and β were the same as those reported in the work of (Smestad et al., 2020). On the other hand, slightly variations were established for γ, being the initial guess set to 0, and the boundary conditions set to $-1 \leq \gamma \leq 1$.

In this study, 4 different 3-wavelengths combinations, which are detailed in the flowchart presented in Fig. 2, are analyzed to model the soiling TPR. To evaluate their accuracy, the modeled profiles are compared with the ones that have been measured using the spectrophotometer, and the error is quantified through different metrics that are presented below.

The mean absolute error (MAE) quantifies the average magnitude of the errors in a set of predictions, regardless of their direction. It is a negatively oriented metric, which means that the lower the better, so a value of 0% reflects that all the modeled data equals the measured ones. The MAE is calculated by the following equation:

$$MAE\,[\%] = \frac{100}{N} \bullet \sum_{i=1}^{N} \left| Z_{mod,i} - Z_{meas,i} \right| \tag{2}$$

where $Z_{mod,i}$ and $Z_{meas,i}$ are the i^{th}-pair of modeled and measured data. N is the total number of pairs.

The mean error (ME) also calculates the average value of the errors between the modeled and the measured data. In contrast to the MAE, its value can be either positive if the modeled data overestimates the measured ones, or negative otherwise. However, although a value of zero indicates no systematic bias, it does not necessarily mean that the modeled data perfectly fit the measured ones. The ME can be obtained by means of the following expression:

$$ME\,[\%] = \frac{100}{N} \bullet \sum_{i=1}^{N} \left(Z_{mod,i} - Z_{meas,i} \right) \tag{3}$$

Last, artificially soiled PV glass coupons are utilized as samples to check the validity of the aforementioned methodology. Soiling deposition is achieved using a self-designed soiling chamber. The procedure of this artificial soiling deposition along the materials employed are detailed in the Appendix.

3. Results and discussion

The results of this study are divided into two sections. The first one covers the modeling of the soiling TPR, whereas the second one presents the estimation of the soiling losses in PV devices of different technologies using these modeled TPRs.

3.1. Soiling transmittance modeling

Spectral hemispherical TPRs have been measured and modeled for each of the soiled glass samples. It should be highlighted that all the TPRs shown in this work refer to relative hemispherical transmittance and express the ratio of the transmittance of the soiled sample to the transmittance of a reference clean sample. Due to this fact, these relative TPRs are called soiling TPRs, as they quantify only the hemispherical attenuation of soiling. Below, the results of using DUSST with different combinations of 3 monochromatic LEDs to model the soiling TPR are presented. Fig. 3 shows the fits for three representative soiling TPRs of samples with different dust accumulations, and the absolute errors between the measured and the modeled profiles as a function of the wavelength. Also, the errors between the measured profiles and two cases of flat profiles, which are generated by assuming that the transmittance does not vary with the wavelength, are included. Furthermore, the modeled flat TPRs returned by combination 4 should be mentioned. This is an expected output and can be accounted for the LEDs measurements of that combination, which are concentrated in a tiny region of the spectrum (448 nm to 591 nm) in comparison with the measurement wavelength range of the spectrophotometer (380 nm to 1080 nm). These modeled flat profiles indicate that combination 4 is not suitable to model the spectral profile of soiling and that should be discarded.

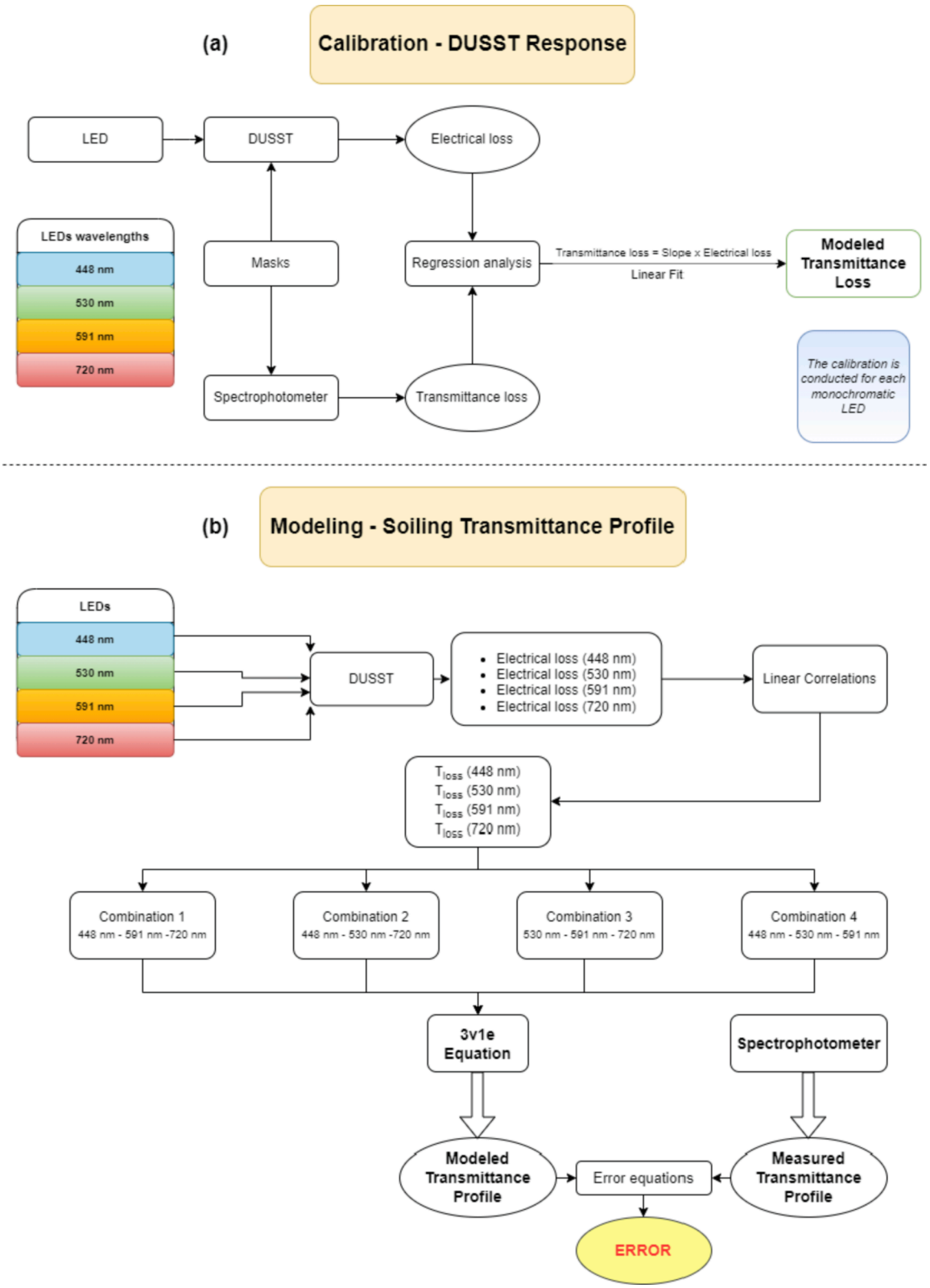

Fig. 2. a) Flowchart of the calibration of the sensor response. b) Flowchart of the soiling TPR modeling.

The accuracy of the different 3-wavelength combinations to model the soiling TPR is assessed through the statistical metrics described before. Fig. 4 compares the measured and the modeled soiling TPRs. It can be clearly appreciated that the magnitude of the MAE for all the models increases with the soiling transmittance losses, as the lower the average transmittance the higher the error. Besides, as it was expected and with the exception of combination 4, which is the only one that does not include a measurement at 720 nm, the values of the MAE with three monochromatic measurements are significantly lower than those returned by assuming a flat profile (higher than 4.5% for transmittance losses greater than 60%). Focusing on the different 3-wavelength combinations, it can be noticed that those that do not include the minimum

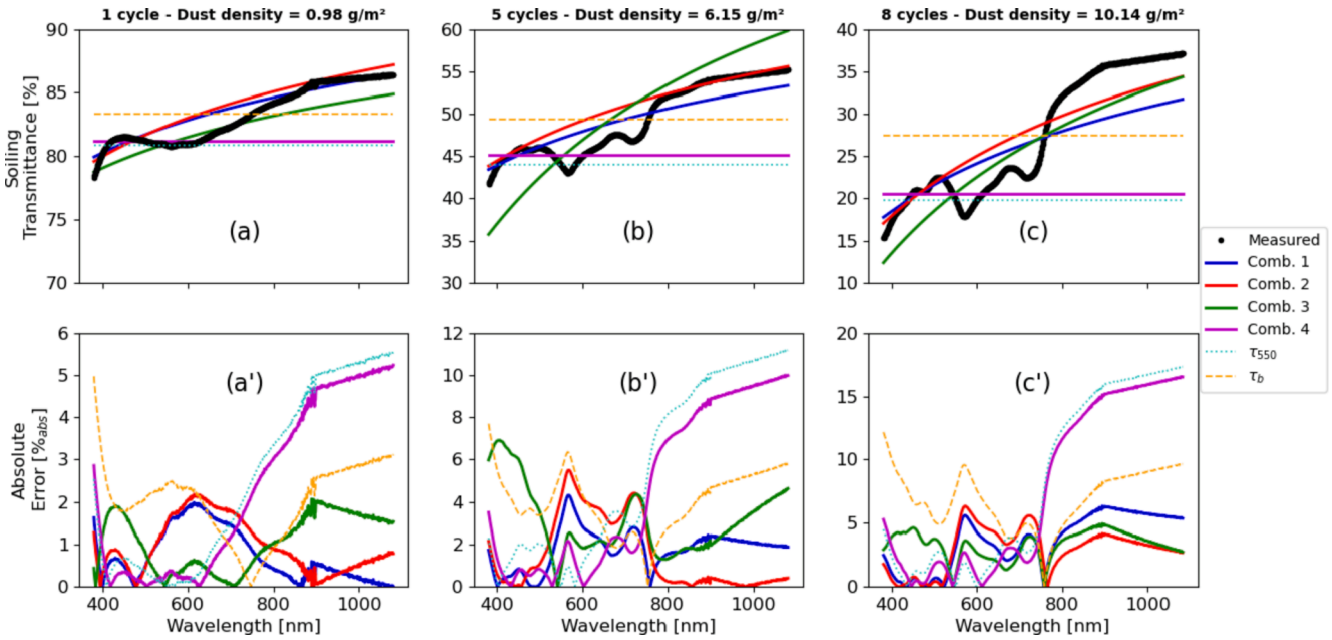

Fig. 3. Plots of the first row: Measured and modeled soiling TPRs using Eq. (1) and the different wavelength combinations shown in Fig. 2. Flat TPRs considering the average (broadband) transmittance (τ_b), and the measured transmittance at 550 nm (τ_{550}) are also included. Plots of the second row: Absolute error for each wavelength between the measured and the modeled transmittance. Three representative samples are shown: (a) and (a'): light soiled, (b) and (b'): moderate soiled, (c) and (c'): heavily soiled. The plots on each column have the same x-axis scale.

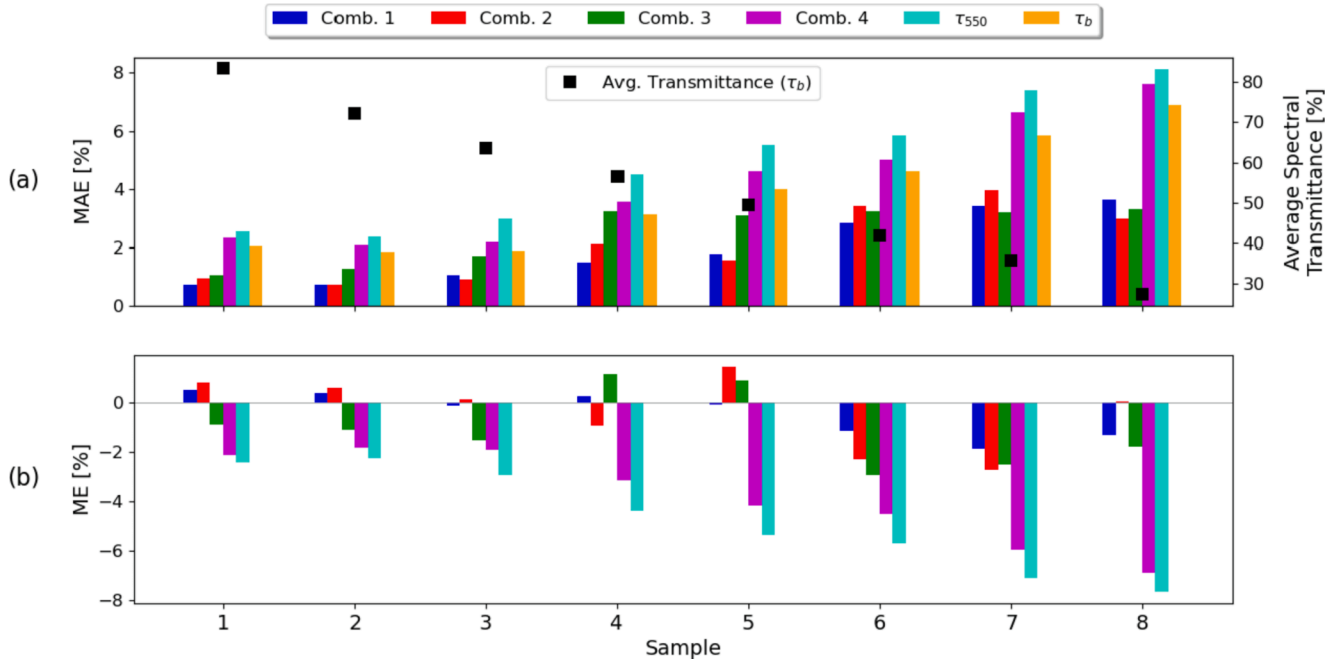

Fig. 4. (a): Mean absolute error (MAE) and (b): mean error (ME) for the different 3-wavelength combinations. Also, the errors associated to the comparison of the measured TPR of the samples with the flat TPRs considering the average (broadband) transmittance (τ_b), and the transmittance at 550 nm (τ_{550}) are included.

or the maximum available wavelength, i.e. a measurement at 448 nm (combination 3) or at 720 nm (combination 4), return higher errors. As an example, for the soiled sample after 2 cycles that presents a dust density of 2.2 g/m^2 and an average transmittance loss of 28.8%, the MAE, which is shown in Fig. 4a, returned by combinations 1 and 2 is 0.7%, whereas the values associated to combinations 3 and 4 are 1.3% and 2.1% respectively, which are almost double and triple. These differences can be explained by the different distribution of the LEDs' wavelengths across the spectrum, as combinations that cover a wider range of the spectrum, such as combinations 1 and 2, are expected to fit better the TPR than those combinations whose LEDs are concentrated in a narrower range, such as combinations 3 and 4. For the three samples with a highest dust density, similar MAE values, between 2.8% and 3.9%, are provided by combinations 1, 2 and 3. This may be due to the synthesis of two factors: (i) the change in the shape of the measured TPR as it can be appreciated in both plots b and c of Fig. 3, being this fact more accentuated in Fig. 3c, and, (ii) the very similar modeled TPRs returned by these combinations because they all include the

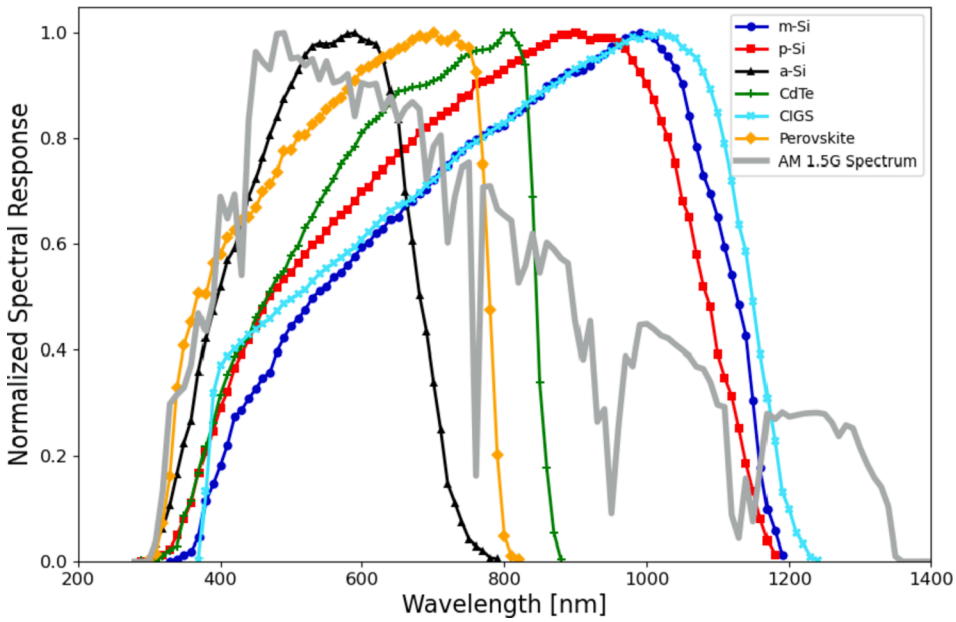

Fig. 5. Normalized spectral response of different PV technologies and normalized AM 1.5G reference spectrum. The PV technologies are: monocrystalline silicon (m-Si), polycrystalline silicon (p-Si), amorphous silicon (a-Si), cadmium-telluride (CdTe), copper-indium-gallium-selenide (CIGS) and perovskite. The normalized spectral response data were sourced from a recent study (Fernández-Solas et al., 2021).

measurement at the maximum available wavelength (720 nm).

Regarding the mean error, which is plotted in Fig. 4b, a clear overestimation of the transmittance losses (high negative ME values) can be seen if only a single wavelength measurement, 550 nm in this case, is considered. This fact is also reflected when combination 4 is applied, because its three measurements are concentrated in a narrow wavelength range (448 nm to 591 nm), where the soiling impacts more the transmittance and the PV performance. The other three combinations return ME values (less than 3%) that do not indicate the presence of systematic bias.

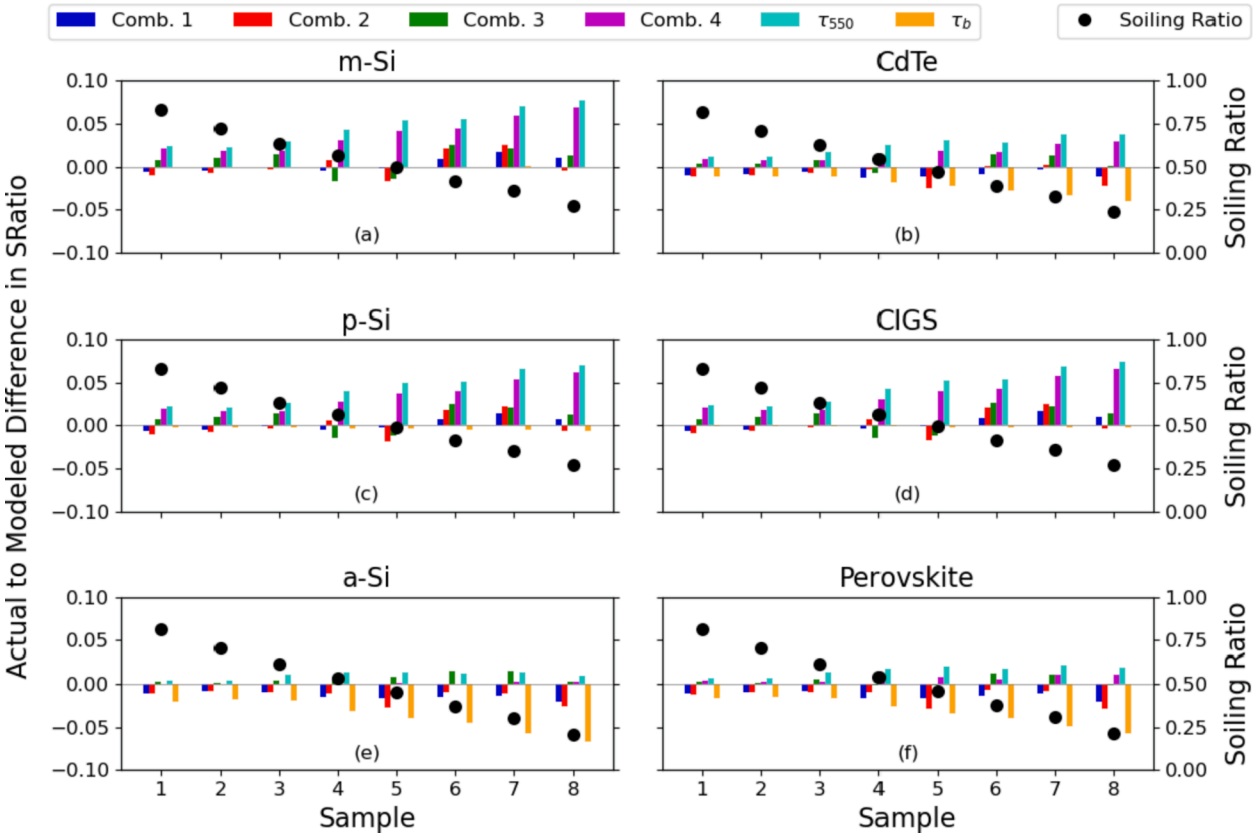

Fig. 6. Difference between the soiling ratio, SRatio, calculated with the measured soiling TPRs and the SRatio obtained through the different modeled profiles presented in Section 3.1 for six different PV technologies. The plots on each row have the same y-axis scale.

3.2. Photovoltaic soiling losses estimation

Herein, the modeled soiling TPRs presented in the previous section are used to estimate the electrical losses of PV modules of different technologies. Due to the differences in the spectral response of the distinct PV technologies, which can be appreciated in Fig. 5, the same transmittance losses do not necessarily translate into identical electrical losses for all of them. The soiling losses have been quantified through the soiling ratio (SRatio) metric, which represents the ratio of the short-circuit currents (Isc) of a soiled to a clean reference PV device. The lower its value the higher the soiling losses, as these are given by 1 – SRatio. The following equation is used to calculate the SRatio:

$$SRatio = \frac{\mathrm{Isc_{soiled}}}{Isc_{ref}} = \frac{\int_{\lambda_{min}}^{\lambda_{max}} \mathrm{E_G}(\lambda) \bullet \tau(\lambda) \bullet SR(\lambda) \bullet d\lambda}{\int_{\lambda_{min}}^{\lambda_{max}} \mathrm{E_G}(\lambda) \bullet SR(\lambda) \bullet d\lambda} \quad (4)$$

where $E_G(\lambda)$ is the standard air mass (AM) 1.5 global spectrum (W m^{-2} nm^{-1}) (NREL, n.d.), $\tau(\lambda)$ is the soiling hemispherical transmittance, and $SR(\lambda)$ is the spectral response of the PV cells that comprised the module and that varies with the PV material. λ_{max} and λ_{min} are, respectively, the longest and the shortest wavelengths (nm) of the device's spectral response. It should be noted that due to the restrictions in the wavelength measurement range of the hemispherical transmittance, the lower and the upper limits are restricted to be $\geq$ 300 nm and $\leq$ 1080 nm, respectively, in this study.

Fig. 6 shows the difference between the SRatio values calculated with measured soiling TPRs and the values obtained with the different modeled profiles presented in the previous section. It can be appreciated that the highest underestimations of the SRatio, i.e. overestimations of the soiling losses, occur when a flat profile with a value equal to the measured transmittance at 550 nm is considered for all the PV technologies, with the exception of amorphous silicon (a-Si) and perovskite, as it can be appreciated in Fig. 6e and in Fig. 6f, respectively. With these technologies, the largest errors (overestimations of the SRatio) are returned if the measured average transmittance (i.e., a flat profile) is utilized in the calculations. It can also be noticed that the use of a flat profile with the value of the average soiling transmittance returns negligible differences (less than 0.01) for monocrystalline silicon (m-Si), polycrystalline silicon (p-Si) and for copper-indium-gallium-selenide (CIGS) technologies. This fact may be accounted for the combination of three factors: (i) the overestimation of the soiling transmittance in the blue and VIS regions of the spectrum, (ii) the underestimation of the transmittance in the infrared region, and (iii) the wide spectral response of these materials. Thus, the excess of losses in the infrared region of the spectrum offsets the losses underestimation in the blue and VIS regions. In this way, the modeled SRatios match the measured ones for the set of samples utilized in this study. However, this cannot be considered always valid, as slight variations in the shape of the TPRs may significantly impact the results. On the other hand, if only the results provided by the use of 3-wavelength measurements to model the transmittance are compared, combinations 1 and 2, which both includes measurements at the shortest (448 nm) and longest wavelength (720 nm) available, returns in average the best results for all the PV technologies. Combination 3, which does not include a measurement at the shortest wavelength, provides also accurate results with differences between the modeled and the measured values less than 0.03, even for the most heavily soiled samples, for those PV technologies with a wide waveband that have their maximum spectral response in the infrared region of the spectrum (m-Si, p-Si and CIGS). As commented above, the use of combination 4, which does not include a measurement in the infrared region, to calculate the SRatio should be avoided because it produces flat soiling TPRs.

4. Conclusions

In this work, the possibility of modeling the spectral profile of soiling transmittance using multiple monochromatic measurements has been experimentally investigated. For this purpose, the DUSST sensor has been modified to measure transmittance at distinct wavelengths. Artificially soiled PV glass coupons with different values of dust density have been used to compare the results returned by four different 3-wavelength combinations. Three of the combinations significantly reduce the error between the measured and the modeled TPRs (MAE less than 4% for all the coupons) when compared to the use of a single wavelength (MAE from 4.5% up to 8.1% for the most heavily soiled samples). The combination that does not include a measurement at the longest wavelength returned major errors, especially in the infrared region of the spectrum, where it significantly overestimated the transmittance losses (errors higher than 15% for transmittance losses of 65%). Also, the electrical losses were estimated for different PV technologies using the modeled soiling TPRs with the different combinations. The results indicate that the best combination of wavelengths depends on the spectral response of the PV technology. This should be taken into account to choose the optimal combination of monochromatic light sources to estimate the soiling losses with the highest accuracy. The results show that for all the examined PV technologies, the use of the most suitable three-wavelength combination significantly improves the SRatio estimation, as no differences between the measured and the modeled SRatio values higher than 0.03 are returned. These errors are significantly lower than those obtained if only a single wavelength measurement at 550 nm is applied. These are indeed greater than 0.05 for the most heavily soiled samples in the case of silicon and thin-film (CdTe and CIGS) technologies.

Future works should consider a wider variety of wavelengths, including measurements in the UV and in the infrared regions of the spectrum, to complement the results presented in this paper. In addition, this innovative optical soiling detection approach should be validated outdoors, under real operation conditions of soiling, by modifying the current version of the DUSST prototype.

Declaration of Competing Interest

The authors declare that they have no known competing financial interests or personal relationships that could have appeared to influence the work reported in this paper.

Acknowledgements

Álvaro Fernández Solas is supported by the Spanish Ministry of Science and Innovation under the program "Ayudas para la formación de profesorado universitario (FPU), 2018 (Ref. FPU18/01460)". Eduardo F. Fernández thanks the Spanish Ministry of Science and Innovation (RYC-2017-21910). Leonardo Micheli is supported by the Spanish Ministry of Science and Innovation under the Ramón y Cajal 2020 program (RYC2020-030094-I) and by Sole4PV, a project funded by the Italian Ministry of University and Research under the 2019 «Rita Levi Montalcini» Program for Young Researchers.

Appendix A. Supplementary data

Supplementary data to this article can be found online at https://doi.org/10.1016/j.solener.2022.06.036.

References

Amano, H., Collazo, R., Santi, C.D., Einfeldt, S., Funato, M., Glaab, J., Hagedorn, S., Hirano, A., Hirayama, H., Ishii, R., Kashima, Y., Kawakami, Y., Kirste, R., Kneissl, M., Martin, R., Mehnke, F., Meneghini, M., Ougazzaden, A., Parbrook, P.J., Rajan, S., Reddy, P., Römer, F., Ruschel, J., Sarkar, B., Scholz, F., Schowalter, L.J., Shields, P., Sitar, Z., Sulmoni, L., Wang, T., Wernicke, T., Weyers, M., Witzigmann, B., Wu, Y.-R., Wunderer, T., Zhang, Y., 2020. The 2020 UV emitter roadmap. J. Phys. D. Appl. Phys. 53 (50), 503001. https://doi.org/10.1088/1361-6463/aba64c.

Ångström, A., Angstrom, A., 1929. On the Atmospheric Transmission of Sun Radiation and on Dust in the Air. Geogr. Ann. 11, 156. https://doi.org/10.2307/519399.

Bessa, J.G., Micheli, L., Almonacid, F., Fernández, E.F., 2021. Monitoring Photovoltaic Soiling: Assessment, Challenges and Perspectives of Current and Potential Strategies. iScience 24 (3), 102165. https://doi.org/10.1016/j.isci.2021.102165.

Burton, P.D., Hendrickson, A., Ulibarri, S.S., Riley, D., Boyson, W.E., King, B.H., 2016. Pattern Effects of Soil on Photovoltaic Surfaces. IEEE J. Photovoltaics 6 (4), 976–980. https://doi.org/10.1109/JPHOTOV.2016.2567100.

Burton, P.D., King, B.H., 2014. Spectral sensitivity of simulated photovoltaic module soiling for a variety of synthesized soil types. IEEE J. Photovoltaics 4 (3), 890–898. https://doi.org/10.1109/JPHOTOV.2014.2301895.

Burton, P.D., King, B.H., Riley, D., 2015. Predicting the spectral effects of soils on high concentrating photovoltaic systems. Sol. Energy 112, 469–474. https://doi.org/10.1016/j.solener.2014.11.022.

Chanchangi, Y.N., Ghosh, A., Baig, H., Sundaram, S., Mallick, T.K., 2021. Soiling on PV performance influenced by weather parameters in Northern Nigeria. Renew. Energy 180, 874–892. https://doi.org/10.1016/j.renene.2021.08.090.

Costa, S.C.S., Diniz, A.S.A.C., Kazmerski, L.L., 2018. Solar energy dust and soiling R&D progress: Literature review update for 2016. Renew. Sustain. Energy Rev. https://doi.org/10.1016/j.rser.2017.09.015.

Deceglie, M.G., Micheli, L., Muller, M., 2018. Quantifying Soiling Loss Directly from PV Yield. IEEE J. Photovoltaics 8 (2), 547–551. https://doi.org/10.1109/JPHOTOV.2017.2784682.

Einhorn, A., Micheli, L., Miller, D.C., Simpson, L.J., Moutinho, H.R., To, B., Lanaghan, C. L., Muller, M.T., Toth, S., John, J.J., Warade, S., Kottantharayil, A., Engtrakul, C., 2019. Evaluation of soiling and potential mitigation approaches on photovoltaic glass. IEEE J. Photovoltaics 9 (1), 233–239. https://doi.org/10.1109/JPHOTOV.2018.2878286.

Fathi, M., Abderrezek, M., Grana, P., 2017. Technical and economic assessment of cleaning protocol for photovoltaic power plants: Case of Algerian Sahara sites. Sol. Energy 147, 358–367. https://doi.org/10.1016/J.SOLENER.2017.03.053.

Fernández-Solas, Á., Micheli, L., Almonacid, F., Fernández, E.F., 2021. Optical degradation impact on the spectral performance of photovoltaic technology. Renew. Sustain. Energy Rev. 141, 110782. https://doi.org/10.1016/j.rser.2021.110782.

Fernández-Solas, A., Micheli, L., Muller, M., Almonacid, F., Fernández, E.F., 2020. Design, Characterization and Indoor Validation of the Optical Soiling Detector "DUSST". Sol. Energy 211, 1459–1468. https://doi.org/10.1016/j.solener.2020.10.028.

Fernández, E.F., Chemisana, D., Micheli, L., Almonacid, F., 2019. Spectral nature of soiling and its impact on multi-junction based concentrator systems. Sol. Energy Mater. Sol. Cells 201, 110118. https://doi.org/10.1016/j.solmat.2019.110118.

Fernández, E.F., Muller, M.T., Micheli, L., Cruz, F.A., 2020. Methods and systems for determining soiling on photovoltaic devices. 10 (734), 946.

Fernández, E.F., Soria-Moya, A., Almonacid, F., Aguilera, J., 2016. Comparative assessment of the spectral impact on the energy yield of high concentrator and conventional photovoltaic technology. Sol. Energy Mater. Sol. Cells 147, 185–197. https://doi.org/10.1016/j.solmat.2015.12.003.

Figgis, B., Ennaoui, A., Ahzi, S., Remond, Y., 2017. Review of PV soiling measurement methods. In: in: Proceedings of 2016 International Renewable and Sustainable Energy Conference, IRSEC 2016. Institute of Electrical and Electronics Engineers Inc, pp. 176–180. https://doi.org/10.1109/IRSEC.2016.7984027.

Gostein, M., Caron, J.R., Littmann, B., 2014. Measuring soiling losses at utility-scale PV power plants. 2014 IEEE 40th Photovolt. Spec. Conf. PVSC 2014, 885–890. https://doi.org/10.1109/PVSC.2014.6925056.

Gostein, M., Düster, T., Thuman, C., 2015. Accurately Measuring PV Soiling Losses with Soiling Station Employing PV Module Power Measurements. In: in: 2015 IEEE 42nd Photovoltaic Specialist Conference (PVSC), pp. 1–4. https://doi.org/10.1109/PVSC.2015.7355993.

Gostein, M., Faullin, S., Miller, K., Schneider, J., Stueve, B., 2018. Mars Soiling Sensor™, in: 2018 IEEE 7th World Conference on Photovoltaic Energy Conversion, WCPEC 2018 - A Joint Conference of 45th IEEE PVSC, 28th PVSEC and 34th EU PVSEC. Bruxelles, Belgium, pp. 3417–3420. https://doi.org/10.1109/PVSC.2018.8547767.

Ilse, K., Micheli, L., Figgis, B.W., Lange, K., Daßler, D., Hanifi, H., Wolfertstetter, F., Naumann, V., Hagendorf, C., Gottschalg, R., Bagdahn, J., 2019. Techno-Economic Assessment of Soiling Losses and Mitigation Strategies for Solar Power Generation. Joule 3 (10), 2303–2321. https://doi.org/10.1016/j.joule.2019.08.019.

Javed, W., Guo, B., Figgis, B., 2017. Modeling of photovoltaic soiling loss as a function of environmental variables. Sol. Energy 157, 397–407. https://doi.org/10.1016/j.solener.2017.08.046.

John, J.J., Rajasekar, V., Boppana, S., Chattopadhyay, S., Kottantharayil, A., TamizhMani, G., 2015. Quantification and Modeling of Spectral and Angular Losses of Naturally Soiled PV Modules. IEEE J. Photovoltaics 5 (6), 1727–1734. https://doi.org/10.1109/JPHOTOV.2015.2463745.

Kimber, A., Mitchell, L., Nogradi, S., Wenger, H., 2006. The effect of soiling on large grid-connected photovoltaic systems in California and the Southwest Region of the United States. Conf. Rec. 2006 IEEE 4th World Conf. Photovolt. Energy Conversion, WCPEC-4 2, 2391–2395. https://doi.org/10.1109/WCPEC.2006.279690.

Korevaar, M., Mes, J., Nepal, P., Snijders, G., van Mechelen, X., 2017. Novel soiling detection system for solar panels, in: 33rd European Photovoltaic Solar Energy Conference. Amsterdam.

Martín, N., Ruiz, J.M., 2005. Annual angular reflection losses in PV modules. Prog. Photovoltaics Res. Appl. 13 (1), 75–84. https://doi.org/10.1002/pip.585.

Micheli, L., Caballero, J.A., Fernandez, E.F., Smestad, G.P., Nofuentes, G., Mallick, T.K., Almonacid, F., 2019. Correlating photovoltaic soiling losses to waveband and single-value transmittance measurements. Energy 180, 376–386. https://doi.org/10.1016/J.ENERGY.2019.05.097.

Micheli, L., Fernandez, E.F., Muller, M., Almonacid, F., 2020a. Extracting and Generating PV Soiling Profiles for Analysis, Forecasting, and Cleaning Optimization. IEEE J. Photovoltaics 10 (1), 197–205. https://doi.org/10.1109/JPHOTOV.2019.2943706.

Micheli, L., Fernández, E.F., Muller, M., Smestad, G.P., Almonacid, F., 2020b. Selection of optimal wavelengths for optical soiling modelling and detection in photovoltaic modules. Sol. Energy Mater. Sol. Cells 212, 110539. https://doi.org/10.1016/j.solmat.2020.110539.

Micheli, L., Theristis, M., Livera, A., Stein, J.S., Georghiou, G.E., Muller, M., Almonacid, F., Fernandez, E.F., 2021. Improved PV Soiling Extraction Through the Detection of Cleanings and Change Points. IEEE J. Photovoltaics 11 (2), 519–526. https://doi.org/10.1109/JPHOTOV.2020.3043104.

Micheli, L., Theristis, M., Talavera, D.L., Almonacid, F., Stein, J.S., Fernández, E.F., 2020c. Photovoltaic cleaning frequency optimization under different degradation rate patterns. Renew. Energy 166, 136–146. https://doi.org/10.1016/j.renene.2020.11.044.

Muller, M., Micheli, L., Solas, A.F., Gostein, M., Robinson, J., Morely, K., Dooraghi, M., Alghamdi, Y.A., Almutairi, Z.A., Almonacid, F., Fernandez, E.F., 2021. An in-depth field validation of "DUSST": a novel low-maintenance soiling measurement device. Prog. Photovoltaics Res. Appl. 29 (8), 953–967. https://doi.org/10.1002/pip.3415.

NREL, n.d. Reference Solar Spectral Irradiance: Air Mass 1.5 [WWW Document]. URL https://www.nrel.gov/grid/solar-resource/spectra-am1.5.html (accessed 11.8.21).

Qasem, H., Betts, T.R., Müllejans, H., AlBusairi, H., Gottschalg, R., 2014. Dust-induced shading on photovoltaic modules. Prog. Photovolt: Res. Appl. 22 (2), 218–226. https://doi.org/10.1002/pip.2230.

Ravi, P., Muller, M., Simpson, L.J., Choudhary, D., Mantha, S., Subramanian, S., Virkar, S., Curtis, T., Tamizhmani, G., 2019. Indoor Soil Deposition Chamber: Evaluating Effectiveness of Antisoiling Coatings. IEEE J. Photovoltaics 9 (1), 227–232. https://doi.org/10.1109/JPHOTOV.2018.2877021.

Rodrigo, P.M., Gutiérrez, S., Micheli, L., Fernández, E.F., Almonacid, F.M., 2020. Optimum cleaning schedule of photovoltaic systems based on levelised cost of energy and case study in central Mexico. Sol. Energy 209, 11–20. https://doi.org/10.1016/j.solener.2020.08.074.

Saura, J.M., Rodrigo, P.M., Almonacid, F.M., Chemisana, D., Fernández, E.F., 2021. Experimental characterisation of irradiance and spectral non-uniformity and its impact on multi-junction solar cells: Refractive vs. reflective optics. Sol. Energy Mater. Sol. Cells 225, 111061. https://doi.org/10.1016/j.solmat.2021.111061.

Şevik, S., Aktaş, A., 2022. Performance enhancing and improvement studies in a 600 kW solar photovoltaic (PV) power plant; manual and natural cleaning, rainwater harvesting and the snow load removal on the PV arrays. Renew. Energy 181, 490–503. https://doi.org/10.1016/j.renene.2021.09.064.

Skomedal, A., Haug, H., Marstein, E.S., 2019. Endogenous Soiling Rate Determination and Detection of Cleaning Events in Utility-Scale PV Plants. IEEE J. Photovoltaics 9 (3), 858–863. https://doi.org/10.1109/JPHOTOV.2019.2899741.

Smestad, G.P., Germer, T.A., Alrashidi, H., Fernández, E.F., Dey, S., Brahma, H., Sarmah, N., Ghosh, A., Sellami, N., Hassan, I.A.I., Desouky, M., Kasry, A., Pesala, B., Sundaram, S., Almonacid, F., Reddy, K.S., Mallick, T.K., Micheli, L., 2020. Modelling photovoltaic soiling losses through optical characterization. Sci. Rep. 10 (1) https://doi.org/10.1038/s41598-019-56868-z.

Song, Z., Liu, J., Yang, H., 2021. Air pollution and soiling implications for solar photovoltaic power generation: A comprehensive review. Appl. Energy 298, 117247. https://doi.org/10.1016/j.apenergy.2021.117247.

Susilo, N., Ziffer, E., Hagedorn, S., Cancellara, L., Netzel, C., Ploch, N.L., Wu, S., Rass, J., Walde, S., Sulmoni, L., Guttmann, M., Wernicke, T., Albrecht, M., Weyers, M., Kneissl, M., 2020. Improved performance of UVC-LEDs by combination of high-temperature annealing and epitaxially laterally overgrown AlN/sapphire. Photonics Res. 8 (4), 589.

Virtanen, P., Gommers, R., Oliphant, T.E., Haberland, M., Reddy, T., Cournapeau, D., Burovski, E., Peterson, P., Weckesser, W., Bright, J., van der Walt, S.J., Brett, M., Wilson, J., Millman, K.J., Mayorov, N., Nelson, A.R.J., Jones, E., Kern, R., Larson, E., Carey, C.J., Polat, İ., Feng, Y.u., Moore, E.W., VanderPlas, J., Laxalde, D., Perktold, J., Cimrman, R., Henriksen, I., Quintero, E.A., Harris, C.R., Archibald, A. M., Ribeiro, A.H., Pedregosa, F., van Mulbregt, P., Vijaykumar, A., Bardelli, A.P., Rothberg, A., Hilboll, A., Kloeckner, A., Scopatz, A., Lee, A., Rokem, A., Woods, C.N., Fulton, C., Masson, C., Häggström, C., Fitzgerald, C., Nicholson, D.A., Hagen, D.R., Pasechnik, D.V., Olivetti, E., Martin, E., Wieser, E., Silva, F., Lenders, F., Wilhelm, F., Young, G., Price, G.A., Ingold, G.-L., Allen, G.E., Lee, G.R., Audren, H., Probst, I., Dietrich, J.P., Silterra, J., Webber, J.T., Slavič, J., Nothman, J., Buchner, J., Kulick, J., Schönberger, J.L., de Miranda Cardoso, J.V., Reimer, J., Harrington, J., Rodríguez, J.L.C., Nunez-Iglesias, J., Kuczynski, J., Tritz, K., Thoma, M., Newville, M., Kümmerer, M., Bolingbroke, M., Tartre, M., Pak, M., Smith, N.J., Nowaczyk, N., Shebanov, N., Pavlyk, O., Brodtkorb, P.A., Lee, P., McGibbon, R.T., Feldbauer, R., Lewis, S., Tygier, S., Sievert, S., Vigna, S., Peterson, S., More, S., Pudlik, T., Oshima, T., Pingel, T.J., Robitaille, T.P., Spura, T., Jones, T.R., Cera, T., Leslie, T., Zito, T., Krauss, T., Upadhyay, U., Halchenko, Y.O., Vázquez-Baeza, Y., 2020. SciPy 1.0: fundamental algorithms for scientific computing in Python. Nat. Methods 17 (3), 261–272. https://doi.org/10.1038/s41592-019-0686-2.

Zorrilla-Casanova, J., Piliougine, M., Carretero, J., Bernaola-Galván, P., Carpena, P., Mora-López, L., Sidrach-de-Cardona, M., 2013. Losses produced by soiling in the incoming radiation to photovoltaic modules. Prog. Photovoltaics Res. Appl. 21 (4), 790–796. https://doi.org/10.1002/pip.1258.